Scaling Laws and Regime Transitions of Macroturbulence in Dry Atmospheres

TAPIO SCHNEIDER

California Institute of Technology, Pasadena, California

CHRISTOPHER C. WALKER

Department of Earth and Planetary Science, Harvard University, Cambridge, Massachusetts

(Manuscript received 7 September 2007, in final form 5 December 2007)

ABSTRACT

In simulations of a wide range of circulations with an idealized general circulation model, clear scaling laws of dry atmospheric macroturbulence emerge that are consistent with nonlinear eddy–eddy interactions being weak. The simulations span several decades of eddy energies and include Earth-like circulations and circulations with multiple jets and belts of surface westerlies in each hemisphere. In the simulations, the eddy available potential energy and the barotropic and baroclinic eddy kinetic energy scale linearly with each other, with the ratio of the baroclinic eddy kinetic energy to the barotropic eddy kinetic energy and eddy available potential energy decreasing with increasing planetary radius and rotation rate. Mean values of the meridional eddy flux of surface potential temperature and of the vertically integrated convergence of the meridional eddy flux of zonal momentum generally scale with functions of the eddy energies and the energy-containing eddy length scale, with a few exceptions in simulations with statically near-neutral or neutral extratropical thermal stratifications. Eddy energies scale with the mean available potential energy and with a function of the supercriticality, a measure of the near-surface slope of isentropes. Strongly baroclinic circulations form an extended regime in which eddy energies scale linearly with the mean available potential energy. Mean values of the eddy flux of surface potential temperature and of the vertically integrated eddy momentum flux convergence scale similarly with the mean available potential energy and other mean fields.

The scaling laws for the dependence of eddy fields on mean fields exhibit a regime transition between a regime in which the extratropical thermal stratification and tropopause height are controlled by radiation and convection and a regime in which baroclinic entropy fluxes modify the extratropical thermal stratification and tropopause height. At the regime transition, for example, the dependence of the eddy flux of surface potential temperature and the dependence of the vertically integrated eddy momentum flux convergence on mean fields changes—a result with implications for climate stability and for the general circulation of an atmosphere, including its tropical Hadley circulation.

1. Introduction

A theory of the zonally and temporally averaged surface climate of a planet with a dry atmosphere must account for how the mean zonal surface winds and the mean surface temperatures depend on external parameters such as the planetary radius, the planetary rotation rate, and the radiative heating contrast between equator and poles. In the extratropics, where the Rossby number is small, the turbulent boundary layer drag on the mean zonal surface wind at any latitude is approximately balanced by the vertically integrated convergence of the meridional eddy flux of zonal momentum in the atmospheric column above it. To the extent that the turbulent boundary layer drag depends only on the mean surface wind, the vertically integrated eddy momentum flux convergence approximately determines the mean zonal surface wind (Held and Hoskins 1985). In the tropics, the Hadley circulation contributes to the meridional transport of zonal momentum and to the maintenance of the mean zonal surface winds, and its dynamics is also influenced by the divergence of eddy momentum fluxes (Walker and Schneider 2006; Schneider 2006). Thus, the vertically integrated eddy momentum flux convergence is the

Corresponding author address: Tapio Schneider, California Institute of Technology, Mail Code 100-23, 1200 E. California Blvd., Pasadena, CA 91125.
E-mail: tapio@caltech.edu

DOI: 10.1175/2007JAS2616.1

principal eddy field for which a closure needs to be found in a theory of the mean zonal surface winds.

The mean surface temperature or surface potential temperature at any latitude is determined by the atmospheric thermal stratification and a balance of radiative processes, ocean heat flux, and the meridional entropy flux (or, equivalently, the meridional mass flux along isentropes) in the atmospheric column above it. In the tropics, the mass flux along isentropes is primarily that of the Hadley cells. In the extratropics of Earth's atmosphere and of sufficiently baroclinic atmospheres in general, it is primarily associated with eddies, with contributions from the mean meridional circulation, which is in turn related to the convergence of the eddy momentum flux. Because the eddy mass flux along isentropes near the surface scales with a static stability factor and with the meridional eddy flux of surface potential temperature, and because it is related to the eddy mass flux along isentropes in the interior atmosphere by a balance condition, the meridional eddy flux of surface potential temperature is the principal eddy field for which a closure needs to be found in a theory of the mean surface temperatures (Held and Schneider 1999; Schneider 2005).

A minimal theory of the mean surface climate of a planet with a dry atmosphere, then, must account for how the vertically integrated eddy momentum flux convergence and the eddy flux of surface potential temperature depend on external parameters and mean fields such as the meridional surface potential temperature gradient and the thermal stratification of the atmosphere. Both eddy fields are related to the vertically integrated eddy flux of potential vorticity along isentropes: the vertically integrated eddy momentum flux convergence is its barotropic component (associated with meridional momentum transport), and the eddy flux of surface potential temperature is proportional to its baroclinic component (associated with vertical momentum transport by form or pressure drag) (Green 1970; Andrews 1983; Tung 1986; Koh and Plumb 2004; Schneider 2005). See Held (1999) and Schneider (2006, 2007) for introductions to this view of the general circulation of an atmosphere.

This paper presents scaling laws describing how mean values of the eddy flux of surface potential temperature, of the vertically integrated eddy momentum flux convergence, and of other characteristics of atmospheric macroturbulence depend on other eddy fields, on mean fields, and on external parameters. We focus on idealized dry atmospheres with axisymmetric and stationary flow statistics as a prerequisite for considerations of more complex atmospheres with, for example, latent heat release in phase changes of water.

Considerations of how macroturbulence modifies the thermal structure of an atmosphere and how, in turn, it is affected by the thermal structure are key for obtaining macroturbulence scaling laws. We have recently presented a theory and simulations with an idealized GCM showing that in the extratropics of dry atmospheres over a surface, a nondimensional measure of the slope of near-surface isentropes, the supercriticality, cannot substantially exceed one (Schneider and Walker 2006, hereafter SW06). If the differential heating of the surface is weak, baroclinic entropy fluxes are weak, the extratropical thermal stratification and tropopause height are controlled by radiation and convection, and, provided the radiative–convective thermal stratification is statically stable, the supercriticality is less than one. If the differential heating of the surface is sufficiently strong, baroclinic entropy fluxes modify the extratropical thermal stratification, tropopause height, and meridional surface potential temperature gradient in such a way that the supercriticality does not substantially exceed one. As a consequence of this constraint on extratropical thermal structures, nonlinear eddy–eddy interactions and the concomitant inverse energy cascade from the scales of baroclinic instability to larger scales are inhibited, the scale of the energy-containing eddies is similar to the scale of the linearly most unstable baroclinic waves, and the eddy kinetic and available potential energies scale linearly with each other.

We build on these results and use the idealized GCM simulations in SW06 and in an unpublished manuscript of T. Schneider and T. M. Merlis (2008, hereafter SchM), spanning a range of eddy energies several orders of magnitude wider than any previously simulated with GCMs, to derive semiempirical scaling laws of atmospheric macroturbulence. We show that the scaling laws for the dependence of eddy fields on mean fields exhibit a regime transition between a regime in which the extratropical thermal stratification and tropopause height are controlled by radiation and convection and a regime in which baroclinic entropy fluxes modify the extratropical thermal stratification and tropopause height. At the regime transition, for example, the dependence of the eddy flux of surface potential temperature and of the vertically integrated eddy momentum flux convergence on mean fields changes—a result that has implications for climate stability and for the general circulation of an atmosphere, including its tropical Hadley circulation.

Section 2 briefly describes the idealized GCM simulations. Section 3 reviews results of SW06 and SchM and presents the central macroturbulence closure, which relates eddy energies to the mean available potential energy. Sections 4 and 5 develop the eddy en-

ergy closure into closures for mean values of the eddy flux of surface potential temperature and of the vertically integrated eddy momentum flux convergence. Section 6 discusses the implications of the results for climate stability and the general circulation, their relation to previous work, and their limitations and broader applicability. The appendices contain details on an approximation of the mean available potential energy used in this paper and on the estimation of flow statistics from the GCM simulations.

We use the following symbols and notation. Overbars denote zonal and temporal means: $\overline{(\cdot)}$ is a generic mean or a mean along sigma levels if the argument depends on a vertical coordinate; $\overline{(\cdot)}^s$ is a mean along the surface or immediately above a near-surface mixed layer; $\overline{(\cdot)}^\sigma = \overline{(p_s \cdot)}/\overline{p}_s$ is a surface pressure–weighted mean along sigma levels. Primes $(\cdot)'$ denote fluctuations about the respective means. Angle brackets $\langle \cdot \rangle$ denote an area-weighted meridional mean over a baroclinic zone, and curly brackets $\{\cdot\}$ denote an area-weighted meridional mean over the extratropics (between 20° and 90° latitude). Square brackets $[\cdot]$ denote a mass-weighted vertical integral. The subscript s marks surface or near-surface quantities. For simplicity, we often refer to surface and near-surface quantities as surface quantities, with the understanding that, in practice, surface quantities involving potential temperature or velocities are evaluated above any near-surface mixed layer; see appendix B for details.

2. Idealized GCM simulations

The idealized GCM simulations analyzed here are the same as those described in SW06 and SchM. A full description can be found there; a brief overview is given here.

Radiative heating and cooling in the idealized GCM are represented by Newtonian relaxation of temperatures toward radiative equilibrium states that are hemispherically symmetric and, in the lower troposphere, statically unstable. Convective heating and cooling are represented by a quasi-equilibrium convection scheme that relaxes temperatures in an atmospheric column toward a profile with fixed convective lapse rate $\gamma\Gamma_d$ whenever the column is statically less stable than one with lapse rate $\gamma\Gamma_d$, where $\Gamma_d = g/c_p = 9.8\ \mathrm{K\ km^{-1}}$ is the dry adiabatic lapse rate and $\gamma \leq 1$ is a rescaling parameter. For $\gamma = 1$, the convection scheme is a dry convection scheme; for $\gamma < 1$, the convection scheme mimics the stabilization of an atmospheric column by latent heat release in moist convection, with the implied latent heat release increasing with decreasing γ. The convection scheme does not transport momentum. Turbulent mixing in a planetary boundary layer of fixed height (2.5 km) is represented as shear-dependent vertical diffusion of momentum and dry static energy with turbulent Prandtl number one (Smagorinsky et al. 1965). The GCM's lower boundary is homogeneous, thermally insulating, and has a constant roughness length of 5 cm in all but one series of simulations (see below).

With the GCM, we simulated a wide range of circulations for different planetary radii a, planetary rotation rates Ω, convective lapse rates $\gamma\Gamma_d$, and Newtonian relaxation times τ. For an Earth-like convective lapse rate of 6.8 K km^{-1} ($\gamma = 0.7$), we varied the planetary radius and rotation rate between Earth's values (a_e and Ω_e) and values four times larger. For $a = a_e$ and $\Omega = \Omega_e$, we varied the convective lapse rate between 5.9 K km^{-1} ($\gamma = 0.6$) and 9.8 K km^{-1} ($\gamma = 1.0$). In these simulations, the Newtonian relaxation time is 50 days in the interior atmosphere and varies near the surface (on sigma levels with $\sigma > 0.85$) between 7 days at the equator and 50 days at the poles (Schneider 2004). For $a = a_e$, $\Omega = \Omega_e$, and $\gamma = 0.7$, we varied the Newtonian relaxation time between 12.5 and 200 days, using a constant relaxation time throughout the atmosphere. For each setting of these parameters, we generated a series of simulations by varying the pole-to-equator surface temperature contrast in radiative equilibrium (Δ_h) between a minimum of 15, 22.5, or 30 K (whichever value leads to appreciable eddy activity for the given setting of the other parameters) and a maximum of 360 K. We also performed one series of simulations with $a = a_e$, $\Omega = \Omega_e$, $\gamma = 0.7$, and a reduced surface roughness length (0.05 cm). In total, we present results from 223 simulations.

The resolution of the simulations ranges from T42 to T127 in the horizontal, depending on planetary radius and rotation rate, and there are 30 unequally spaced sigma levels in the vertical. All simulation results shown are averages over at least 100 days after a statistically steady state was reached. See SW06 and SchM for a more detailed description of the simulations and an analysis of the extratropical thermal stratifications and Walker and Schneider (2006) for an analysis of the Hadley circulations in some of the series of the simulations.

Figure 1 shows mean fields and eddy fluxes of interest in this paper in two of the simulations, one Earth-like and one with four times Earth's rotation rate and enhanced pole-to-equator temperature contrasts. In the Earth-like simulation (Figs. 1a,c), the zonal wind and potential temperature fields and the structure and magnitude of the meridional eddy flux of potential temperature and of the divergence of the meridional eddy flux of zonal momentum resemble those in Earth's atmosphere. The simulation with four times Earth's ro-

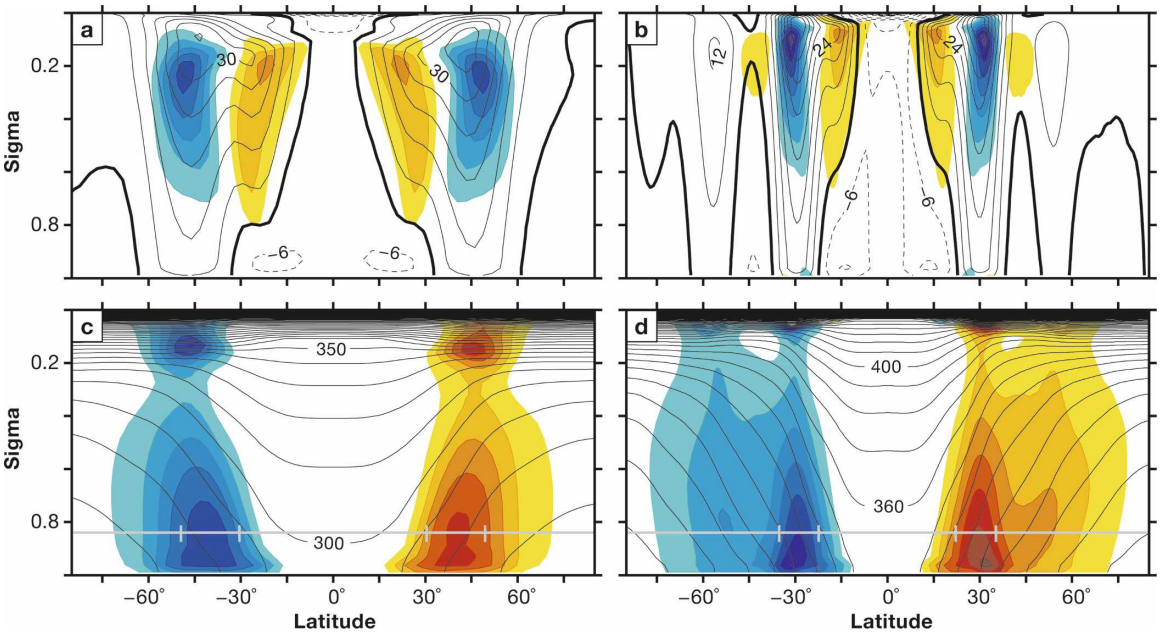

FIG. 1. (a),(b) Mean zonal wind $\overline{u}^{\sigma}$ (contours) and eddy momentum flux divergence $\mathrm{div}(\overline{p}_s\,\overline{u'v'}^{\sigma}\cos\phi)/\overline{p}_s$ (colors) and (c),(d) mean potential temperature $\overline{\theta}^{\sigma}$ (contours) and eddy potential temperature flux $\overline{v'\theta'}^{\sigma}$ (colors) in two idealized GCM simulations. The vertical coordinate is $\sigma = p/p_s$. (a),(c) Simulation with planet radius and rotation rate of Earth ($\Delta_h = 90$ K, $\gamma = 0.7$). (b),(d) Simulation with planet radius of Earth and rotation rate four times that of Earth ($\Delta_h = 180$ K, $\gamma = 0.7$). The contour intervals are 6 m s^{-1} for zonal wind (negative contours dashed and zero contour thick), 10 K for potential temperature, (a) 6×10^{-6} m s^{-2} and (b) 1.8×10^{-5} m s^{-2} for eddy momentum flux divergence, and (c) 4 K m s^{-1} and (d) 6 K m s^{-1} for eddy potential temperature flux. Red tones indicate positive values and blue tones negative values. The gray line indicates the level $\sigma = 0.84$ at which the near-surface eddy potential temperature flux in Fig. 7 is evaluated, with the vertical bars demarcating, for the two simulations shown, the baroclinic zones over which mean fields in Figs. 4–8 and Fig. A1 are averaged.

tation rate exhibits two jets and belts of surface westerlies in each hemisphere (Figs. 1b,d). Forcings and boundary conditions in the GCM are hemispherically symmetric, so the deviations from hemispheric symmetry seen in Fig. 1 are an indication of the sampling variability owing to the finiteness of the averaging period.

The circulation statistics in Fig. 1 exhibit familiar features. Eddy momentum fluxes converge from the flanks into the centers of the jets (Figs. 1a,b), consistent with meridional wave activity propagation away from the jet centers. This is expected for weakly nonlinear eddies on jets such as those in Fig. 1, with meridional widths of order Rossby radius or larger (Held 1975; Held and Andrews 1983; Ioannou and Lindzen 1986; Lee 1997). (There is eddy momentum flux convergence with a maximum of 1.2×10^{-5} m s^{-2} in the center of the second jet in Fig. 1b, but it is too weak to be seen with the contouring in the figure.) For the lowest-latitude ("subtropical") jets, which are the strongest jets when multiple jets are present, the strongest eddy momentum flux divergence occurs, as in Earth's atmosphere, in the equatorward flanks of the jets, consistent with predominantly equatorward propagation of wave activity away from the jet centers. This eddy momentum flux divergence strongly influences the Hadley circulation in many of the simulations (Walker and Schneider 2006). Eddy potential temperature fluxes are poleward throughout the atmosphere, as in Earth's atmosphere, with a maximum near the surface and typically a second maximum near the tropopause (Figs. 1c,d).

The mean and eddy fields in Fig. 1 are of fundamental importance for the general circulation of an atmosphere. A goal of this paper is to show how mean values of these eddy fields are related to eddy energies, eddy length scales, and mean fields.

3. Eddy energy closure

a. *Supercriticality*

In SW06, we showed that large-scale averages of extratropical thermal structures satisfy the constraint that the supercriticality

$$S_c = -\frac{f_0}{\beta_0}\frac{\langle \partial_y \overline{\theta}_s \rangle}{\Delta_v} \tag{1}$$

does not substantially exceed one, where f_0 and β_0 are reference values of the Coriolis parameter and of its derivative. The supercriticality (1) resembles the supercriticality of the quasigeostrophic two-layer model (e.g., Pedlosky 1970; Held and Larichev 1996). However, the surface potential temperature gradient $\partial_y \overline{\theta}_s$ appears in it in place of the vertically averaged potential temperature gradient in the two-layer model, and the bulk stability,

$$\Delta_v = -2\langle \overline{\partial_p \theta}^s \rangle \langle \overline{p}_s - \overline{p}_t \rangle, \tag{2}$$

with surface pressure $\overline{p}_s$ and tropopause pressure $\overline{p}_t$, involves a static stability at or near the surface, $-\overline{\partial_p \theta}^s$, in place of a vertically averaged static stability appearing in the two-layer model. Also, whereas an inviscid quasigeostrophic two-layer model is baroclinically stable if its supercriticality is less than one, $S_c < 1$ does not imply that an atmosphere is baroclinically stable.

As discussed in SW06, the supercriticality is a nondimensional measure of the slope of near-surface isentropes. It is also a ratio $S_c \sim \langle \overline{p}_s - \overline{p}_e \rangle / \langle \overline{p}_s - \overline{p}_t \rangle$ of two pressure differences: that between the surface and the level ($\overline{p}_e$) up to which baroclinic entropy fluxes extend, and that between the surface and the tropopause. In the limit of small surface potential temperature gradients, baroclinic entropy fluxes are weak, and the extratropical thermal stratification and tropopause height are controlled by radiation and convection. In this limit, provided the radiative–convective thermal stratification is statically stable, baroclinic entropy fluxes do not extend to the tropopause, such that $\langle \overline{p}_e \rangle > \langle \overline{p}_t \rangle$ and $S_c < 1$. This corresponds to the shallow-wave limit discussed by Held (1978a) in the context of quasigeostrophic theory. In the limit of large surface potential temperature gradients, baroclinic entropy fluxes modify the extratropical thermal stratification and tropopause height and extend to the tropopause. In this limit, the pressure range over which baroclinic eddies redistribute entropy defines the troposphere (Held 1982; Schneider 2004), such that $\langle \overline{p}_e \rangle \sim \langle \overline{p}_t \rangle$ and $S_c \sim 1$. The net result is the constraint $S_c \lesssim 1$ on extratropical thermal structures.

We found the constraint $S_c \lesssim 1$ to be well satisfied in the idealized GCM simulations considered here, with consequences for properties of the macroturbulence (SW06; SchM). For example, Fig. 2 shows spectra of the barotropic eddy kinetic energy for two simulations with twice Earth's radius, one with $S_c < 1$ ($\Delta_h = 22.5$ K) and one with $S_c \sim 1$ ($\Delta_h = 90$ K). The spectra are typical of the simulations in general, both in that they exhibit a power-law range with an approximate n^{-3} or somewhat steeper scaling with spherical wavenumber n and also in that the Rossby wavenumbers are similar to the energy-containing wavenumbers.[1] The Rhines wavenumber is larger than the energy-containing wavenumber for $S_c < 1$ and similar to the energy-containing wavenumber for $S_c \sim 1$. The energy-containing wavenumber is larger in the simulation with $S_c < 1$ than in the simulation with $S_c \sim 1$, and this is also evident in instantaneous flow fields. For example, Fig. 3 shows the potential vorticity on isentropes at instants in the statistically steady states of the simulations in Fig. 2. The isentropes lie in the midtroposphere in the tropics and cross the tropopause in the extratropics. Wave breaking and potential vorticity filaments at the tropopause and the different length scales of the energy-containing eddies in the two simulations are evident. See SW06 for further discussion of characteristic eddy length scales and O'Gorman and Schneider (2007) for further discussion of the shape of the energy spectra. Our macroturbulence closure builds on the constraint $S_c \lesssim 1$ and consequences such as those manifest in Figs. 2 and 3.

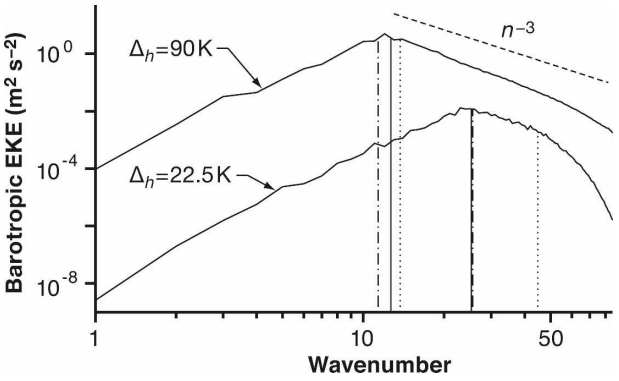

FIG. 2. Spectrum of barotropic eddy kinetic energy for two simulations with $a = 2a_e$, $\gamma = 0.7$, and with $\Delta_h = 22.5$ K and $\Delta_h = 90$ K. The horizontal axis is the spherical wavenumber n. Vertical lines indicate characteristic wavenumbers: Rossby (dashed–dotted), energy-containing (solid), and Rhines (dotted) wavenumbers, computed and with nondimensional constants as in SW06. (The vertical lines for the Rossby and energy-containing wavenumbers are almost indistinguishable for the simulation with $\Delta_h = 22.5$ K.) The dashed line indicates an n^{-3} power law.

b. *Relation between eddy energy and mean available potential energy*

The macroturbulence closure relates eddy energies to the mean available potential energy and to the supercriticality, which both depend only on mean fields.

[1] Only the two simulations with smallest barotropic eddy kinetic energy (see Fig. 5) do not exhibit an approximate n^{-3} power-law range but have only a narrow range of wavenumbers with appreciable eddy kinetic energy, with a steep decay at larger and smaller wavenumbers.

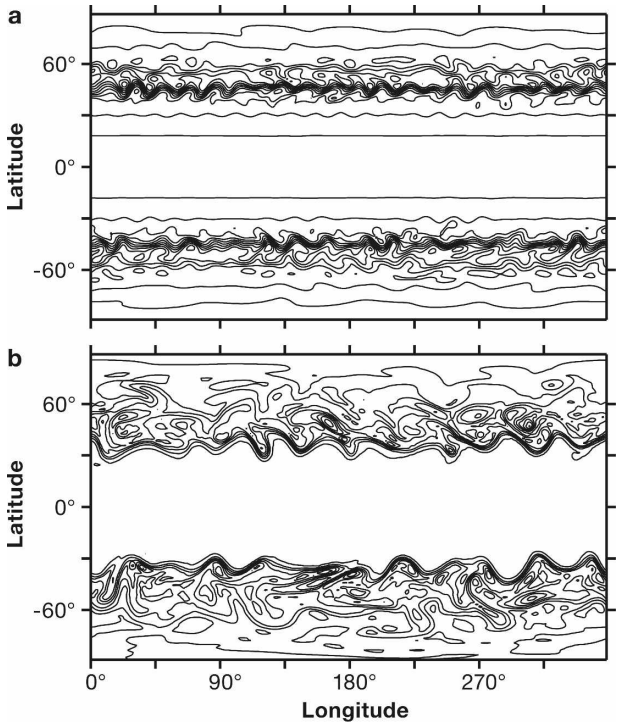

FIG. 3. Instantaneous potential vorticity on isentropes in the simulations in Fig. 2. (a) Simulation with $\Delta_h = 22.5$ K and potential vorticity on 275-K isentrope (contour interval is 0.2 PVU with 1 PVU $\equiv 10^{-6}$ K m^2 kg^{-1} s^{-1}). (b) Simulation with $\Delta_h = 90$ K and potential vorticity on 320-K isentrope (contour interval is 0.8 PVU).

In energy-balance models for a planet's surface climate, it is desirable to express eddy fluxes in terms of surface quantities or quantities that can be estimated from them. We therefore approximate the mean available potential energy (MAPE) per unit area in a baroclinic zone of meridional width L_z by

$$\mathrm{MAPE}_a = \frac{c_p\langle \overline{p}_s - \overline{p}_t\rangle}{24g}\,\Gamma_s\langle \partial_y \overline{\theta}_s\rangle^2 L_z^2, \tag{3}$$

where

$$\Gamma_s = -\frac{\kappa}{p_0}\langle \overline{\partial_p \theta}^s\rangle^{-1} \tag{4}$$

is an inverse measure of the static stability at or near the surface, p_0 is a reference surface pressure, and $\kappa = R/c_p$ is the adiabatic exponent. The approximate mean available potential energy (3) can be obtained from Lorenz's (1955) quadratic expression for the mean available potential energy based on potential temperature variations on pressure or sigma surfaces by Taylor expansion and by approximating the potential temperature gradient and static stability in the troposphere by their surface values. See appendix A for details and for a demonstration of the accuracy of the approximation in the simulations. Using the supercriticality (1) and the approximate mean available potential energy (3) in a macroturbulence closure yields a closure in which eddy energies depend only on mean fields at the surface and on the tropopause pressure, which can be estimated from mean fields at the surface if one assumes, as in the approximation (3), that the static stability does not vary strongly in the vertical within the troposphere (Held 1982; Thuburn and Craig 2000; Schneider 2007).

Our macroturbulence closure relates the eddy available potential energy (EAPE) to the approximate mean available potential energy,

$$\mathrm{EAPE} \sim \mathrm{MAPE}_a \times \xi(S_c), \tag{5}$$

where $\xi(S_c)$ is a monotonically increasing function of the supercriticality, with normalization convention $\xi(1) = 1$. The constraint $S_c \lesssim 1$ then implies $\xi \lesssim 1$. For $S_c \ll 1$, the closure (5) implies EAPE $\ll$ MAPE, consistent with baroclinic entropy fluxes that extend only over a fraction of the troposphere being inefficient at converting mean available potential energy into eddy energy (Held 1978a). For $S_c \sim 1$, the closure (5) reduces to EAPE $\sim$ MAPE$_a$ (cf. Green 1970).

Figure 4 shows the eddy available potential energy as a function of the approximate mean available potential energy in the idealized GCM simulations.[2] The mean fields entering the approximate mean available potential energy (3), and all other mean fields in what follows, are averaged over baroclinic zones that are determined based on the magnitude of the near-surface eddy flux of potential temperature. The length scale L_z is the meridional width of the so-determined baroclinic zones. The boundaries of the baroclinic zones for the two simulations shown in Fig. 1 are marked by the gray vertical bars in that figure. See appendix B for conventions for the determination of baroclinic zones and for the sensitivity of our results to them. Eddy available potential energies, and all other eddy fields in what follows, are averaged between 20° and 90° latitude in both (statistically identical) hemispheres. For most simulations, eddy fields could be averaged globally without substantially changing the results; restricting the averages to latitudes poleward of 20° helps to avoid singularities in low latitudes arising in the computation of the eddy available potential energy in simulations with statically near-neutral or neutral convective lapse

[2] The figures in SW06 include a simulation with $\Delta_h = 15$ K and $a = 2a_e$, which has essentially axisymmetric circulations in which the extremely weak eddy activity is dominated by unsteady dynamics near the GCM's rigid-lid upper boundary. This simulation is not included in Fig. 4 and in subsequent figures in this paper.

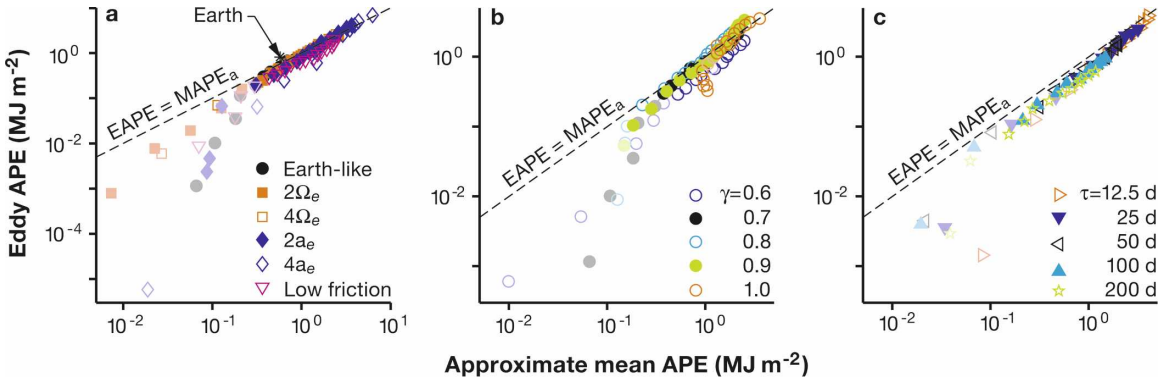

FIG. 4. EAPE vs approximate MAPE. (a) Earth-like simulations with terrestrial rotation rate Ω_e and radius a_e, simulations with two and four times the rotation rate and radius of Earth, and simulations with low frictional drag in the planetary boundary layer (roughness length of surface reduced by a factor of 100). The convective lapse rate is 0.7 Γ_d = 6.8 K km^{-1} in all simulations. (b) Simulations with $a = a_e$, $\Omega = \Omega_e$, and with different convective lapse rates $\gamma\Gamma_d$ (γ = 0.6, . . . , 1.0). The series of simulations with γ = 0.7 in (b) is the same as the series labeled Earth-like in (a). (c) Simulations with $a = a_e$, $\Omega = \Omega_e$, γ = 0.7, and with different Newtonian relaxation times τ. For each set of parameters, the figure shows a series of simulations obtained by varying the radiative-equilibrium surface temperature contrast Δ_h. Pale plotting symbols mark the simulations in which the supercriticality, estimated as in SW06 and SchM, is less than 90% of the value in the simulation with the largest Δ_h in the corresponding series. Here and in subsequent figures, the corresponding quantities for Earth's atmosphere (annual means according to reanalysis data averaged over both hemispheres, marked by an asterisk) are shown for comparison (see appendix B). The dashed lines represent the identity EAPE = MAPE$_a$.

rate. Eddy fields could also be averaged over the baroclinic zones over which mean fields are averaged without substantially changing the results.

Figure 4 shows that, for sufficiently large surface potential temperature gradients and mean available potential energies, all simulations approximately condense onto the linear relation EAPE = MAPE$_a$. This is consistent with the closure (5) and with the result of SW06 and SchM that, for sufficiently large surface potential temperature gradients, all simulations satisfy $S_c \sim 1$. For small surface potential temperature gradients and mean available potential energies, Fig. 4 indicates EAPE < MAPE$_a$, consistent with the closure (5) and $\xi(S_c) < 1$ for $S_c < 1$.[3] The simulations in which the supercriticality, estimated as in SW06 and SchM, is less than 90% of the value in the simulation with the largest Δ_h in the corresponding series are identified by pale plotting symbols. Figure 4 shows that, for each series of simulations, the simulations with EAPE < MAPE$_a$ are generally the simulations in which the supercriticality is less than the $O(1)$ saturation value for the series. Exceptions are a few simulations with a statically neutral convective lapse rate (γ = 1.0) and low surface potential temperature gradients, for which the static stability near the surface is nearly zero and EAPE and MAPE$_a$ are poorly defined. The eddy available potential energy and mean available potential energy in Earth's atmosphere in the annual mean (not taking moisture effects into account) are likewise comparable with each other, with a ratio EAPE/MAPE$_a \approx 1.17$ similar to that in the simulations in the regime EAPE $\sim$ MAPE$_a$ (Fig. 4a).

The scaling of the eddy available potential energy with the mean available potential energy thus is in two regimes: (i) A regime EAPE < MAPE$_a$, in which $S_c < 1$ and the extratropical thermal stratification and tropopause height are controlled by radiation and convection; (ii) a regime EAPE $\sim$ MAPE$_a$, in which $S_c \sim 1$ and baroclinic entropy fluxes modify the extratropical thermal stratification and tropopause height.

The form of the function $\xi(S_c)$ for $S_c < 1$ could in principle be determined from results such as those in Fig. 4. However, the value of the supercriticality in simulations with small surface potential temperature gradients depends too strongly on how the mean fields entering the supercriticality are averaged to allow us to determine the function $\xi(S_c)$ reliably. In identifying simulations with supercriticalities less than 90% of the saturation value for a given series of simulations, we estimated the supercriticalities as in SW06 and SchM, although mean fields in those papers were averaged over wider baroclinic zones than in the present paper (see appendix B for details). Choosing the narrower baroclinic zones of the present paper generally gives somewhat higher supercriticalities for simulations with small surface potential temperature gradients and hence gives somewhat different functional forms for ξ.

[3] Inequalities here and in what follows are to be understood in a scaling sense, that is, after nondimensional $O(1)$ factors have been fixed on the right-hand sides.

Smoothing the boundaries of the baroclinic zones, as well as the latitudes at which the reference values f_0 and β_0 are evaluated, across variations in Δ_h within each series of simulations (SW06; SchM) also affects supercriticalities for simulations with small surface potential temperature gradients. With these caveats, near the transition from the regime with $S_c < 1$ to the regime with $S_c \sim 1$, the function ξ appears to be of the form $\xi \approx S_c^r$ with exponent $r = 4 \pm 1$; however, for smaller surface potential temperature gradients and smaller supercriticalities, the dependence on the supercriticality appears to be stronger. For example, as Δ_h is increased from 30 to 60 K in the series of simulations with $a = 4a_e$, the eddy available potential energy increases by almost four orders of magnitude, while both the approximate mean available potential energy and the supercriticality change only by $O(1)$ factors (see the two simulations with lowest EAPE for $a = 4a_e$ in Fig. 4a). This points to the existence of critical potential temperature gradients for baroclinic instability, which may be an artifact of the vertical discretization in the GCM. The ambiguities in the choice of averaging regions and the questions about the influence of the vertical discretization on our results for the smallest surface potential temperature gradients prevent us from making more precise statements about the form of the function ξ.

The function ξ in the closure (5) can depend on external parameters, such as the planetary radius or rotation rate and radiative or frictional parameters. Figure 4c reveals that there is a weak dependence on the Newtonian relaxation time. The ratio $\mathrm{EAPE/MAPE}_a$ decreases by about a factor of 1.7 for the simulations with the largest values of Δ_h as the Newtonian relaxation time is increased from $\tau = 12.5$ to 200 days. The saturation value of the supercriticality decreases by a similar factor (SchM), suggesting that the decrease in the ratio $\mathrm{EAPE/MAPE}_a$ may be related. On the other hand, the ratio $\mathrm{EAPE/MAPE}_a$ decreases more weakly if the mean available potential energy is averaged over wider baroclinic zones. For example, it decreases by only a factor of 1.3 if baroclinic zones are determined as in SchM—which leaves the significance of the decrease unclear. Systematic dependences on other external parameters are not evident in the figure. For sufficiently large surface potential temperature gradients and mean available potential energies, the simulations with different planetary radii and rotation rates and with reduced surface roughness length appear to collapse onto the closure (5), without explicit dependence on these parameters (or with a dependence too weak to be apparent). However, our exploration of the dependence of the closure (5) on frictional parameters obviously is not exhaustive and cannot rule out explicit dependences on them.

c. Relations among eddy energies

Closures for other eddy energies can be obtained from the closure (5) by relating the other eddy energies to the eddy available potential energy. In the linearly most unstable baroclinic waves, eddy available potential energy and barotropic and baroclinic eddy kinetic energy are equipartitioned (i.e., they scale linearly with each other). Nonlinear eddy–eddy interactions can modify eddy scales and the partitioning among eddy energies (Charney 1971; Rhines 1975; Salmon 1980, 1982), but in quasigeostrophic models, strong nonlinear eddy–eddy interactions require that the quasigeostrophic counterparts of the supercriticality satisfy $S_c \gg 1$ (Pedlosky 1970, 1979; Held and Larichev 1996). The constraint $S_c \lesssim 1$ on extratropical thermal structures suggests that nonlinear eddy–eddy interactions are weak and that macroturbulent eddies in dry atmospheres exhibit the same equipartitioning of eddy energies as the linearly most unstable baroclinic waves (SW06).

Figure 5 shows the barotropic eddy kinetic energy ($\mathrm{EKE}_{\mathrm{bt}}$) as a function of the eddy available potential energy. Over the entire range of climates simulated, spanning several decades of eddy energies, the simulation results indeed collapse approximately onto the linear relation $\mathrm{EAPE} = \mathrm{EKE}_{\mathrm{bt}}$. Simulations with statically near-neutral or neutral convective lapse rates ($\gamma = 0.9$ and 1.0) exhibit anomalously large eddy available potential energies, particularly for small surface potential temperature gradients and eddy available potential energies, for which the stabilization of the extratropical thermal stratification by baroclinic entropy fluxes is weak (Fig. 5b). These anomalies are caused by vanishing or small static stabilities near the surface, where the parameterized mixing of dry static energy in the planetary boundary layer tends to reduce the static stability toward zero. The anomalies largely disappear when levels within the planetary boundary layer are excluded from the computation of the eddy available potential energy. The ratio of eddy available potential energy to barotropic eddy kinetic energy in Earth's atmosphere ($\mathrm{EAPE/EKE}_{\mathrm{bt}} \approx 0.8$) is similar to that in the simulations (Fig. 5a).[4]

[4] The ratio $\mathrm{EAPE/EKE}_{\mathrm{bt}}$ can be larger than one in simulations with a small planetary rotation rate ($\Omega \lesssim \Omega_e/4$), large pole-to-equator temperature contrasts, and strong equatorial superrotation if regions within the Hadley cells are included in the computation of eddy energies (T. M. Merlis 2007, personal communication).

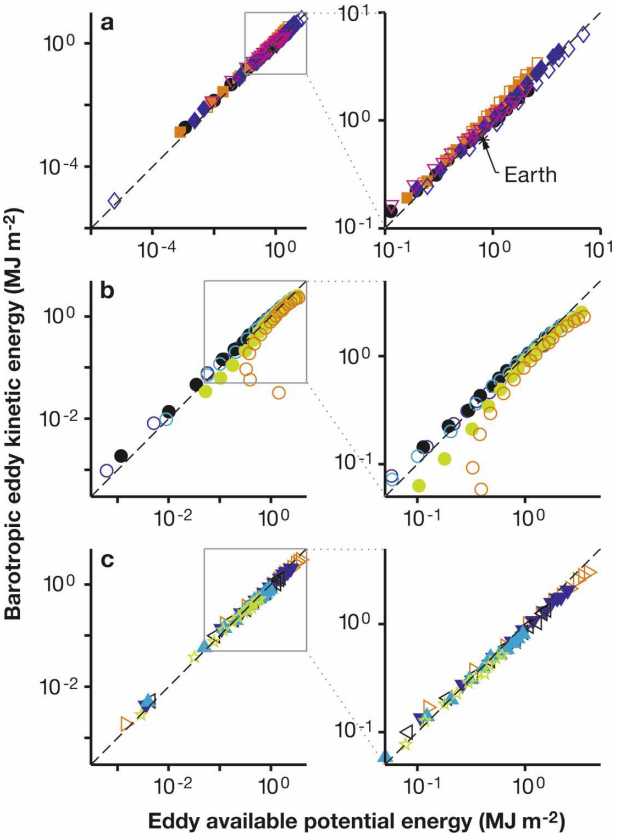

FIG. 5. EKE_{bt} vs EAPE. The dashed lines represent the identity EAPE = EKE_{bt}. Plotting symbols as in Fig. 4.

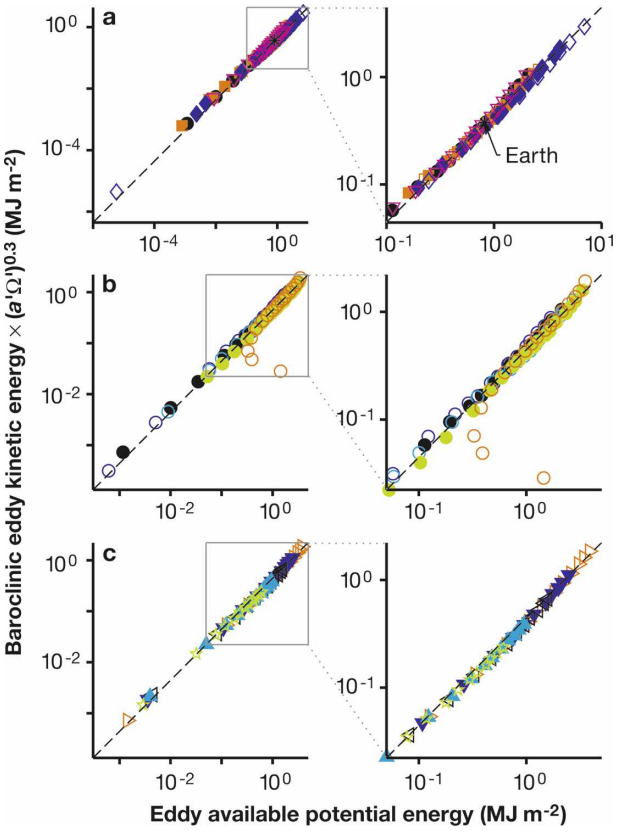

FIG. 6. Rescaled EKE_{bc} vs EAPE. The dashed lines represent the linear relation EAPE = $2.25(a'\Omega')^{0.3}$ EKE_{bc}. Plotting symbols as in Fig. 4.

Figure 6 shows the baroclinic eddy kinetic energy (EKE_{bc}), rescaled by the factor $(a'\Omega')^{0.3}$ with $a' = a/a_a$ and $\Omega' = \Omega/\Omega_e$, as a function of the eddy available potential energy. The baroclinic eddy kinetic energy and eddy available potential energy likewise scale linearly with each other.[5] Their ratio exhibits a dependence on planetary radius and rotation rate, scaling roughly as $EAPE/EKE_{bc} \sim (a'\Omega')^{0.3}$. Whether this ratio indeed obeys a power law in $a'\Omega'$, and if so, with what exponent, cannot be determined unambiguously from the simulations. Power laws with exponents roughly between 0.2 to 0.5 are consistent with the simulation results.

The baroclinic eddy kinetic energy is smaller than the barotropic eddy kinetic energy and the eddy available potential energy. The simulation results collapse approximately onto the linear relation EAPE = $2.25(a'\Omega')^{0.3}$ EKE_{bc}. A few exceptions are again simulations with a statically neutral convective lapse rate ($\gamma = 1.0$), for which eddy available potential energies are anomalously large (Fig. 6b). The anomalies again disappear if levels within the planetary boundary layer are excluded from the computation of the eddy available potential energy (SW06). As for the barotropic eddy kinetic energy, the ratio of eddy available potential energy to baroclinic eddy kinetic energy in Earth's atmosphere ($EAPE/EKE_{bc} \approx 2.2$) is similar to that in the simulations (Fig. 6a).

The equipartitioning EAPE ~ EKE_{bt} is consistent with nonlinear eddy–eddy interactions being weak. However, one would also expect this equipartitioning if eddy–eddy interactions were strong and engendered an inverse energy cascade (Held and Larichev 1996). That the equipartitioning EAPE ~ EKE_{bt} is seen in the simulations may therefore not be surprising, although it is still striking that it is seen so clearly over such a wide range of eddy energies. The equipartitioning EAPE ~ EKE_{bc} is likewise consistent with nonlinear eddy–eddy

[5] Results similar to those in Fig. 6 are contained in SW06 and SchM. Figure 6 differs from the corresponding figures in these other papers in that the averaging conventions for eddy energies differ and in that it makes the dependence of the ratio EAPE/EKE_{bc} on planetary radius and rotation rate explicit.

interactions being weak. If eddy–eddy interactions were strong and engendered a substantial inverse energy cascade, one would expect EAPE $\sim$ EKE$_{bt} \gg$ EKE$_{bc}$ (Held and Larichev 1996; see also Vallis 2006, chapter 9.3). The equipartitioning EAPE $\sim$ EKE$_{bc}$ therefore is evidence that nonlinear eddy–eddy interactions are weak and an inverse energy cascade beyond the scale of the linearly most unstable baroclinic waves is inhibited (SW06). This gives a self-consistent picture: in SW06, we showed that if $S_c \lesssim 1$ and EKE$_{bt} \lesssim$ MAPE$_a$, as implied by the closure (5) and by the equipartitioning EKE$_{bt} \sim$ EAPE, and provided that the relevant baroclinic zone width L_z in the approximate mean available potential energy (3) does not exceed eddy length scales, as is reasonable to assume given that the relevant mean available potential energy is that accessible to eddies, then the Rhines scale is smaller than or at most similar to the Rossby radius (e.g., Fig. 2). Therefore, the energy-containing eddy length scale is similar to the Rossby radius, an inverse energy cascade is inhibited, and nonlinear eddy–eddy interactions are weak.

We presently do not have an explanation for the dependence of the ratios EAPE/EKE$_{bc} \sim$ EKE$_{bt}$/EKE$_{bc}$ on the planetary radius and rotation rate. The dependence does not seem to be related to the ratio of domain size to the scale of the energy-containing eddies, and thus to the number of jets in each hemisphere and to the room for a potential inverse energy cascade. Like simulations with an increased planetary radius and rotation rate, some simulations with Earth's radius and rotation rate exhibit small energy-containing eddies and multiple jets in each hemisphere, without exhibiting a significantly different EAPE/EKE$_{bc}$ ratio than Earth-like simulations with larger energy-containing eddies and only one jet in each hemisphere (see also SW06; Schneider 2006).

With the scaling laws relating the eddy available potential energy to the mean available potential energy and the eddy energies to each other, we can now derive closures for mean values of eddy fluxes.

4. Eddy flux of surface potential temperature

To derive a closure for the mean eddy flux of surface potential temperature, we decompose the mean eddy flux into a correlation coefficient and rms fluctuations,

$$\left\{\overline{v_s'\theta_s'}\right\} = c_\theta \left\{\overline{v_s'^2}\right\}^{1/2} \left\{\overline{\theta_s'^2}\right\}^{1/2}. \tag{6}$$

Averaged over all simulations, for mean values $\{\cdot\}$ of eddy fields between 20° and 90° latitude as before, the so-defined correlation coefficient between near-surface meridional velocity and potential temperature fluctuations is $c_\theta \approx 0.52$. The correlation coefficient varies among the series of simulations, and it varies within series, generally (but not always monotonically) decreasing with increasing Δ_h within a series.[6] However, both the among-series and within-series variations are relatively small. The among-series standard deviation of the series-mean correlation coefficients is 0.06, and the within-series standard deviations of the correlation coefficients for individual simulations are of similar magnitude. Given the accuracy of the closure (5) and of the other scaling laws, these variations are negligible, and we take the correlation coefficient to be constant in what follows.

The rms fluctuations in near-surface meridional velocity and potential temperature can be related to eddy energies through

$$\left\{\overline{v_s'^2}\right\} \sim \mu_t^{-1} \text{EKE}_{bt} \tag{7a}$$

and

$$\left\{\overline{\theta_s'^2}\right\} \sim (\mu_t c_p \Gamma_s)^{-1} \text{EAPE}, \tag{7b}$$

where Γ_s is the inverse static stability measure (4) and $\mu_t = \langle \overline{p}_s - \overline{p}_t \rangle / g$ is the mass per unit area of the troposphere. That is, we assume that the meridional velocity variance and the potential temperature variance near the surface scale with eddy energies per unit mass vertically averaged over the troposphere, that contributions from the troposphere dominate the column-integrated eddy energies, and that the near-surface static stability is the relevant static stability for obtaining the potential temperature variance near the surface from the eddy available potential energy. For the mean eddy flux of surface potential temperature (6), this leads to the scaling law

$$\left\{\overline{v_s'\theta_s'}\right\} \sim \mu_t^{-1} \sqrt{(c_p \Gamma_s)^{-1} \text{EKE}_{bt} \times \text{EAPE}}. \tag{8}$$

In anticipation of substituting mean energies for the eddy energies in this scaling law, we have chosen a static stability Γ_s^{-1} and a mass per unit area of the troposphere μ_t that involve mean values $\langle \cdot \rangle$ over baroclinic zones, as we use for mean fields, rather than mean values $\{\cdot\}$ over the entire extratropics, as we use for eddy fields. Which mean value is chosen for these quantities does not substantially affect the results. Similarly, a ver-

[6] One would expect the correlation coefficient to decrease with increasing ratio of thermal damping time to Lagrangian velocity autocorrelation time (e.g., Swanson and Pierrehumbert 1997). An increase in this ratio through a decrease in the Lagrangian velocity autocorrelation time as Δ_h is increased may be responsible for the decrease in the correlation coefficient within series of simulations.

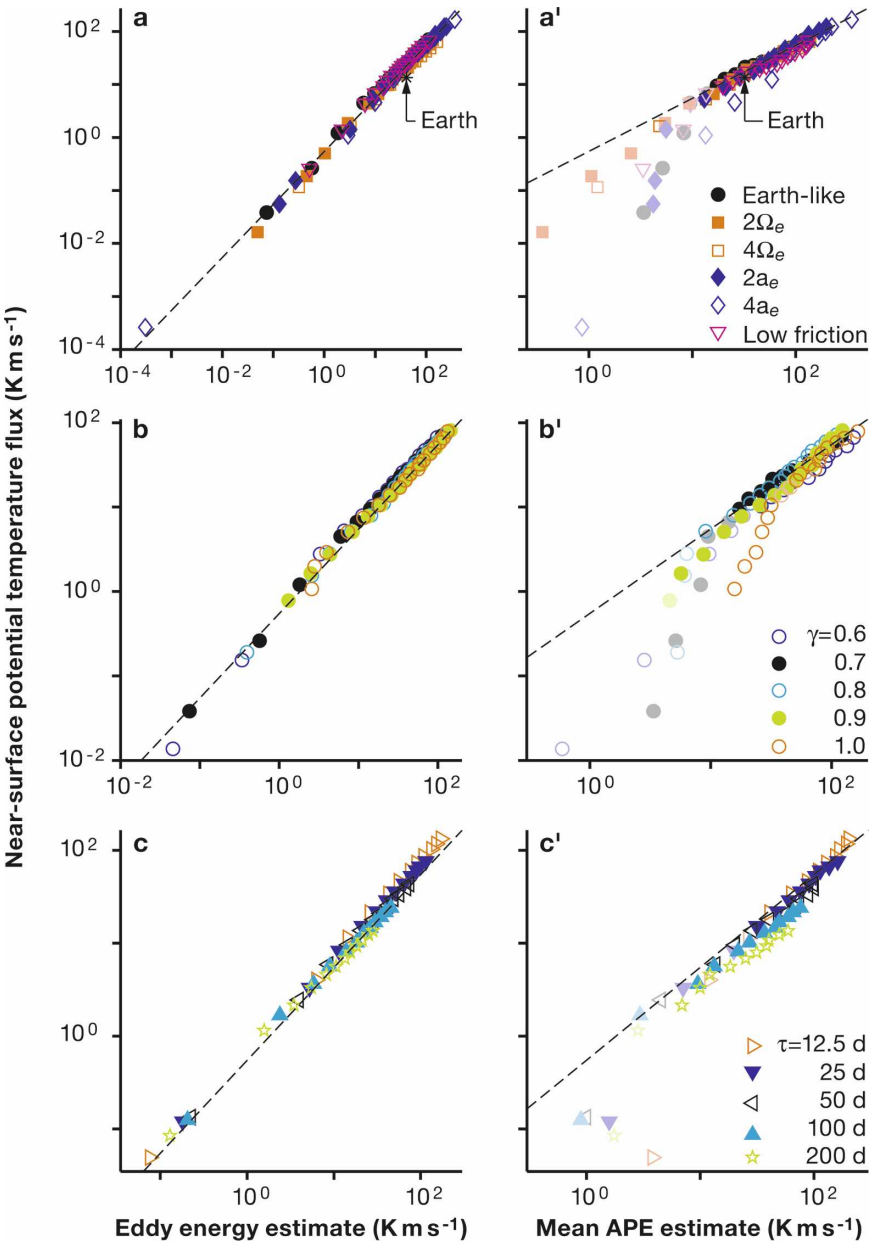

FIG. 7. Mean near-surface eddy flux of potential temperature vs scaling estimates from eddy and mean energies. (a)–(c) Estimate (8) from eddy energies. (a′)–(c′) Estimate (9) with $\xi \equiv 1$ from MAPE. The near-surface eddy flux of potential temperature is evaluated at $\sigma = 0.84$ (gray line in Fig. 1). The dashed lines represent linear relations with slope 0.55. Plotting symbols as in Fig. 4, with pale symbols again marking the simulations in which the supercriticality is less than 90% of the value in the simulation with the largest Δ_h.

tically averaged static stability can be used in place of the near-surface static stability Γ_s^{-1} without substantially affecting the results.

Figures 7a–c show that the scaling law (8) captures the variations of the mean eddy flux of surface potential temperature (more precisely, the mean near-surface eddy flux of potential temperature). The empirical proportionality factor in the scaling law (8)—the quotient of the left-hand side and the right-hand side—is about 0.55. However, particularly for larger Δ_h and larger eddy energies, the proportionality factor varies among the series of simulations with different Newtonian relaxation times (Fig. 7c). It decreases from about 0.77 to about 0.56 as the Newtonian relaxation time is in-

creased from $\tau = 12.5$ to 200 days.[7] This decrease primarily comes about because the analogous proportionality factor in the scaling law (7a) for the meridional velocity variance near the surface decreases with increasing Newtonian relaxation time; that is, the relative contribution of near-surface meridional velocity fluctuations to the barotropic eddy kinetic energy decreases with increasing Newtonian relaxation time.

The motivation for using the barotropic eddy kinetic energy in the scaling law (8) is empirical. The vertical structure of the eddy potential temperature flux (e.g., Figs. 1c,d) suggests that the meridional velocity fluctuations that effect the flux have a substantial barotropic component. Moreover, the baroclinic eddy kinetic energy exhibits an explicit dependence on planetary radius and rotation rate (Fig. 6a), whereas no dependence of this sort is evident for the barotropic eddy kinetic energy (Fig. 5a) or for the mean eddy flux of surface potential temperature (Fig. 7a). As a consequence, using the barotropic eddy kinetic energy in the scaling law (8) gives a better fit to the simulation results than using the baroclinic eddy kinetic energy, without the need to introduce explicit dependences on external parameters. Using the total eddy kinetic energy (which is dominated by the barotropic component) gives comparable results and would also have been justifiable.

If one substitutes the equipartitioning relation $\mathrm{EKE}_{\mathrm{bt}} \sim \mathrm{EAPE}$ and the closure (5) for the eddy energies in the scaling law (8), one obtains a closure for the mean eddy flux of surface potential temperature in terms of mean fields at the surface and the tropopause pressure,

$$\left\{\overline{v_s'\theta_s'}\right\} \sim \mu_t^{-1}(c_p\Gamma_s)^{-1/2}\,\mathrm{MAPE}_a \times \xi(S_c). \qquad (9)$$

Figures 7a′–c′ show the mean eddy flux of surface potential temperature as a function of the right-hand side of this closure, using $\xi \equiv 1$ in the absence of knowledge of the form of the function ξ.

The figure reflects the compound effects of the various scaling laws leading to (9). For example, as for the scaling of the eddy available potential energy with the mean available potential energy, the scaling of the mean eddy flux of surface potential temperature with the mean available potential energy and the other mean fields in the closure (9) is in two regimes, one with $S_c < 1$ (note the pale plotting symbols in Figs. 7a′–c′) and one with $S_c \sim 1$. The mean eddy flux of surface potential temperature in Earth's atmosphere is consistent with the closure (9) in the regime $S_c \sim 1$, here as in the scaling laws leading to (9), with a similar $O(1)$ proportionality factor as for the simulations (Fig. 7a′).

Where the simulation results deviate from the closure (9) or exhibit parameter dependences not made explicit in it, the deviations and parameter dependences are likewise a compound effect of the previously discussed deviations and parameter dependences in the scaling laws leading to (9). For example, the variation with Newtonian relaxation time of the proportionality factor in the closure (9) in the regime $S_c \sim 1$ (Fig. 7c′) is a compound effect of the variation with Newtonian relaxation time of the ratio $\mathrm{EAPE/MAPE}_a$ (Fig. 4c) and of the proportionality factor in the scaling law (8) (Fig. 7c).

While we have focused on the eddy flux of surface potential temperature, the scaling laws derived here are also applicable to the vertically integrated eddy flux of potential temperature. In the simulations, the vertically integrated eddy flux of potential temperature scales with the near-surface eddy flux of potential temperature and is usually dominated by it (see Figs. 1c,d). The fit of the scaling laws to mean values of the vertically integrated eddy flux is similar to the fit to the mean values of the near-surface eddy flux.

5. Vertically integrated eddy momentum flux convergence

A closure for a mean value of the vertically integrated eddy momentum flux convergence can be derived in a similar way as the closure for the mean eddy flux of surface potential temperature. In a mass-weighted global integral, the divergence

$$M_y \equiv \mathrm{div}(\overline{p}_s\,\overline{u'v'}^{\sigma}\cos\phi)/\overline{p}_s$$

of the meridional eddy flux of zonal momentum is zero. To obtain mean values of the vertically integrated divergence or convergence that are representative of large-scale averages, we consider mean values of the mass-weighted vertical integral $[\cdot]$ of the convergence $-\{[M_y^-]\}$, setting divergent contributions to zero:

$$M_y^- = \begin{cases} M_y & \text{if} \quad M_y < 0, \\ 0 & \text{otherwise.} \end{cases}$$

We refer to the mean value $-\{[M_y^-]\}$ as the mean eddy momentum flux convergence.

[7] This decrease is not primarily caused, as one might suspect (cf. footnote 6), by a decrease of the correlation coefficient between near-surface meridional velocity and potential temperature fluctuations. If one excludes simulations with $\Delta_h \le 30$ K, which can have weak eddies and anomalously large correlation coefficients, the series-mean correlation coefficients for the series with different Newtonian relaxation times exhibit only a minimal decrease from $c_\theta \approx 0.58$ for $\tau = 12.5$ days to $c_\theta \approx 0.54$ for $\tau = 50$ days and exhibit no significant further decrease as the Newtonian relaxation time is increased further.

For a global mean $\{\cdot\}$, the mean eddy momentum flux convergence would be equal and opposite to the global-mean eddy momentum flux divergence. For the meridional mean $\{\cdot\}$ between 20° and 90° latitude that we use to average simulation results, it is still approximately proportional to minus the global-mean eddy momentum flux divergence in most simulations, with a constant of proportionality equal to the inverse of the area fraction of the globe included in the average, and with typical deviations from exact proportionality of less than a percent and not exceeding a few percent. Exceptions are simulations with statically near-neutral or neutral convective lapse rates ($\gamma = 0.9$ and 1.0), in which the meridional mean does not include the entire subtropical jet and its associated region of eddy momentum flux convergence, and/or simulations that have substantial equatorial eddy momentum flux convergence. Aside from these, there is only one simulation ($a = 4a_e$, $\Delta_h = 90$ K) in which the meridional mean does not include the entire subtropical jet and misses about 20% of the total eddy momentum flux convergence (see Walker and Schneider 2006, their Figs. 8e, f). In all other simulations, the meridional mean includes essentially all eddy momentum flux convergence, which is usually dominated by the convergence associated with the dominant jet (the subtropical jet if multiple jets are present in each hemisphere).

The mean eddy momentum flux convergence can be related to the baroclinic eddy kinetic energy and the length scale L_e of the energy-containing eddies through

$$-\{[M_y^-]\} \sim \mathrm{EKE}_{\mathrm{bc}}/L_e. \tag{10}$$

That is, we assume that the vertically integrated eddy momentum flux scales with the baroclinic eddy kinetic energy and that it varies meridionally on the energy-containing eddy length scale, which sets the meridional scale of jets and of their associated regions of eddy momentum flux convergence (Panetta 1993; Lee 2005; Schneider 2006; O'Gorman and Schneider 2008a).

Figures 8a–c show the mean eddy momentum flux convergence as a function of the right-hand side of the scaling law (10), using as the length scale L_e the energy-containing scale of the barotropic eddy kinetic energy, defined as a global-mean scale following SW06. (Using the energy-containing scale of the total eddy kinetic energy or that of the baroclinic eddy kinetic energy does not substantially change the results.) The scaling law (10) generally captures the variations of the mean eddy momentum flux convergence, with an empirical proportionality factor of about 0.5. However, particularly for smaller Δ_h and smaller eddy energies, the simulations with statically near-neutral or neutral convective lapse rates ($\gamma = 0.9$ or 1.0) deviate from the scaling law (10), apparently for a complex of reasons. The facts that these simulations, unlike others, exhibit substantial eddy momentum flux convergence in the equatorial region and that their Hadley cells are less strongly influenced by eddy momentum flux divergence than the Hadley cells in other simulations with substantial baroclinic eddy activity (Walker and Schneider 2006) probably play a role in causing the deviations from the scaling law (10).

As for using the barotropic eddy kinetic energy in the scaling law (8) for the mean eddy flux of surface potential temperature, the motivation for using the baroclinic eddy kinetic energy in the scaling law (10) for the mean eddy momentum flux convergence is empirical. The vertical structure of the eddy momentum flux convergence (e.g., Figs. 1a,b) suggests that the velocity fluctuations that effect the momentum flux are predominantly baroclinic. If the barotropic or total eddy kinetic energy is used in a scaling law similar to (10), the implied proportionality factor exhibits a dependence on planetary radius and rotation rate, scaling roughly as $(a'\Omega')^{-0.3}$. No such dependence is evident if the baroclinic eddy kinetic energy is used (Fig. 8a), consistent with the equipartitioning relation $\mathrm{EKE}_{\mathrm{bt}} \sim (a'\Omega')^{0.3}\,\mathrm{EKE}_{\mathrm{bc}}$ (see section 3c). Using the baroclinic eddy kinetic energy in the scaling law (10) therefore gives a better fit to the simulation results without the need to introduce additional parameter dependences.

To obtain a closure for the mean eddy momentum flux convergence from the scaling law (10), one needs a relation between the energy-containing eddy length scale and mean fields. We use the result of SW06 and SchM that because of the weakness of nonlinear eddy–eddy interactions, the energy-containing eddy length scale is similar to the Rossby radius L_R, except when the Rossby radius is so large that the finite size of the planet appears to affect the energy-containing scale, in which case the energy-containing scale is smaller than the Rossby radius. Substituting $L_e \sim L_R$, the equipartitioning relation $\mathrm{EKE}_{\mathrm{bc}} \sim (a'\Omega')^{-0.3}\,\mathrm{EAPE}$, and the closure (5) in the scaling law (10) leads to the closure

$$-\{[M_y^-]\} \sim (a'\Omega')^{-0.3}\,\mathrm{MAPE}_a \times \xi(S_c)/L_R. \tag{11}$$

We estimate the Rossby radius from the near-surface static stability and the tropopause pressure, so the right-hand side of this closure again depends on mean fields at the surface and the tropopause pressure. To account for the fact that the Rossby radius can be larger than the energy-containing eddy length scale when the

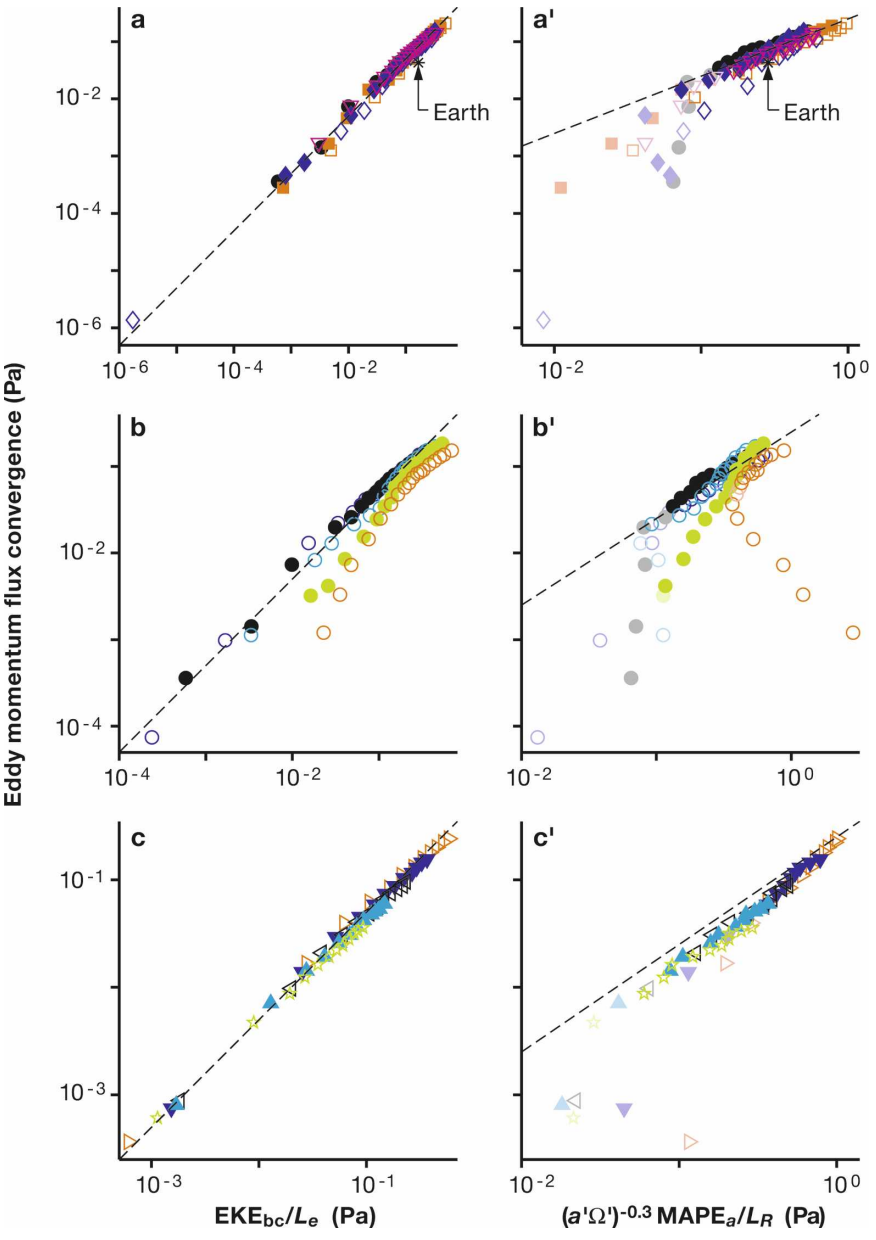

FIG. 8. Mean eddy momentum flux convergence vs scaling estimates from eddy and mean energies. (a)–(c) Estimate (10) from eddy kinetic energy and energy-containing eddy length scale. (a′)–(c′) Estimate (11) with $\xi \equiv 1$ from MAPE and Rossby radius. The dashed lines represent linear relations with (a)–(c) slope 0.50 and (a′)–(c′) slope 0.25. Plotting symbols as in Fig. 7.

finite size of the planet affects the energy-containing scale, we truncate the Rossby radius at the length scale corresponding to spherical wavenumber 4.5 when it exceeds that length scale; see appendix B for details on the computation of the Rossby radius.

Figures 8a′–c′ show the mean eddy momentum flux convergence as a function of the right-hand side of the closure (11), again using $\xi \equiv 1$ in the absence of knowledge of the form of the function ξ. Similarly to Fig. 7 for the mean eddy flux of surface potential temperature, Fig. 8 reflects the compound effects of the scaling laws leading to (11). The scaling of the mean eddy momentum flux convergence with the mean available potential energy and the Rossby radius is again in two regimes, one with $S_c < 1$ (note the pale plotting symbols in Figs. 8a′–c′) and one with $S_c \sim 1$. And the mean eddy momentum flux convergence in Earth's atmosphere is again consistent with the closure (11) in the regime $S_c \sim 1$,

with a similar $O(1)$ proportionality factor as for the simulations.

Deviations from the scaling law (11) are likewise compound effects of the previously discussed deviations in the scaling laws leading to (11). For the simulations with a statically neutral convective lapse rate ($\gamma = 1.0$), the compound effect of the deviations from the respective scaling laws seen in Figs. 4b, 6b, and 8b and of the deviations of the Rossby radius from the energy-containing length scale (SW06) amounts to a breakdown of the scaling law (11). It even gives an incorrect qualitative dependence of the mean eddy momentum flux convergence on mean fields for smaller Δ_h and smaller eddy momentum flux convergence (note that $S_c \sim 1$ in all simulations with $\gamma = 1.0$). In other simulations, however, the scaling law (11) does capture the variations of the mean eddy momentum flux convergence at least in the regime $S_c \sim 1$. The accuracy with which the scaling law (11) is obeyed is limited in large part because the accuracy of the Rossby radius as an estimate of the energy-containing length scale is limited, particularly at large scales (large Δ_h). Our ad hoc truncation of the Rossby radius at large scales only partially mitigates this problem.

6. Discussion and implications

a. Regime transitions

At the transition between the regime $S_c < 1$, in which the extratropical thermal stratification and tropopause height are controlled by radiation and convection, and the regime $S_c \sim 1$, in which baroclinic entropy fluxes modify the extratropical thermal stratification and tropopause height, the dependence of eddy fields on mean fields changes. The scaling laws for the dependence of eddy fields on mean fields involve the product $\mathrm{MAPE}_a \times \xi(S_c)$. Restricted to the dependence on the surface potential temperature gradient and the static stability and with a power law $\xi \sim S_c^r$ for the function ξ, this product scales as

$$\mathrm{MAPE}_a \times S_c^r \sim \begin{cases} \Gamma_s^{r+1} \langle \partial_y \overline{\theta}_s \rangle^{r+2} & \text{if} \quad S_c < 1, \\ \langle \partial_y \overline{\theta}_s \rangle & \text{if} \quad S_c \sim 1, \end{cases} \tag{12}$$

where we have used $S_c \sim \Gamma_s \langle \partial_y \overline{\theta}_s \rangle$. The relation (12) does not fit the simulation results quantitatively because the dependences suppressed in it, for example, on the tropopause pressure, are important to account for the simulation results. However, the relation (12) illustrates that the dependence of $\mathrm{MAPE}_a \times \xi(S_c)$ on the surface potential temperature gradient and on the static stability changes qualitatively at the transition between the regimes. In the regime $S_c < 1$, $\mathrm{MAPE}_a \times \xi(S_c)$ depends explicitly on the static stability (controlled by convection) and depends strongly nonlinearly on the surface potential temperature gradient (as mentioned in section 3b, the exponent $r = 4 \pm 1$ is consistent with the simulation results near the transition). In the regime $S_c \sim 1$, the explicit dependence on the static stability can be eliminated, and $\mathrm{MAPE}_a \times \xi(S_c)$ depends linearly on the surface potential temperature gradient.

The change in the dependence of $\mathrm{MAPE}_a \times \xi(S_c)$ on the surface potential temperature gradient and on the static stability implies similar changes in the dependence of eddy fields on these mean fields at the regime transition. Consider, for example, the mean eddy flux of surface potential temperature and the mean eddy momentum flux convergence. In the regime $S_c < 1$, they depend explicitly on the convective lapse rate and depend strongly nonlinearly on the surface potential temperature gradient and thus on the mean available potential energy (Figs. 7a′–c′ and 8a′–c′). In the regime $S_c \sim 1$, they do not depend explicitly on the convective lapse rate and depend more weakly on the surface potential temperature gradient and thus on the mean available potential energy. In this regime, the mean eddy flux of surface potential temperature, following the same reasoning as in Eq. (12), scales as $\langle \partial_y \overline{\theta}_s \rangle^{3/2}$. This is roughly consistent with the scaling of the column-integrated eddy flux of sensible heat with the surface potential temperature gradient over a seasonal cycle in midlatitudes of Earth's atmosphere (Stone and Miller 1980). The mean eddy momentum flux convergence, using the expression (B2) for the Rossby radius, scales as $\langle \partial_y \overline{\theta}_s \rangle^{1/2}$. Climate stability implications of the different scalings in the two regimes are discussed below.

b. General circulation

As outlined in the introduction, the eddy flux of surface potential temperature and the eddy momentum flux convergence are of fundamental importance for the surface climate of a planet and for the general circulation of its atmosphere. The closure (9) relating the mean eddy flux of surface potential temperature to mean fields can be used in an energy-balance model for a planet's surface climate to determine the extratropical mean temperatures vertically averaged over the troposphere and, given the static stability, the extratropical mean surface temperatures. The closure (11), relating the mean eddy momentum flux convergence to mean fields, can be used to determine the extratropical mean zonal surface wind, provided that turbulent boundary layer drag can be modeled as depending only on the mean surface wind and other mean fields at the surface. For the function $\xi(S_c)$ in these closures, a power law $\xi = S_c^r$ with exponent $r = 4 \pm 1$ may be a starting

point for qualitative studies of the dependence of the extratropical surface climate on external parameters. The static stability required in such studies can be taken to be the greater of a convective static stability and the static stability consistent with $S_c \sim 1$, such that the constraint $S_c \lesssim 1$ is satisfied.

Beyond the extratropical surface climate, the closure (11) for the mean eddy momentum flux convergence also has implications for the tropical Hadley circulation. In Walker and Schneider (2006), we showed that eddy momentum flux divergence can strongly influence the strength of Hadley cells. In most of the simulations considered here—the principal exceptions being simulations with statically near-neutral or neutral convective lapse rates or with very small surface potential temperature gradients (see Walker and Schneider 2006, their Fig. 6)—the Coriolis force on the mass flux in the upper branches of the Hadley cells, near their center, is primarily balanced by eddy momentum flux divergence; that is, the effective Rossby number of the Hadley cells is small. The simulations in which this balance approximately holds generally are the simulations in which, as discussed in section 5, the global-mean eddy momentum flux divergence is proportional to the mean eddy momentum flux convergence that we considered. Moreover, the global-mean divergence is dominated by the divergence in the equatorward flanks of the subtropical jets—the divergence that influences the Hadley circulation (see Fig. 1 for an example). The implication is that, in those simulations, the strength of the Hadley cells scales with the mean eddy momentum flux convergence, with some modifications resulting from variations in the extent of the Hadley cells that affect the relevant value of the Coriolis parameter linking the Hadley cell mass flux and the eddy momentum flux divergence. The strength of the Hadley cells exhibits the same regime transition as the mean eddy momentum flux convergence, with the dependence of the Hadley cell strength on the surface potential temperature gradient changing at the transition (Walker and Schneider 2006). Coupled to a scaling law for the extent of the Hadley cells and thus for the relevant value of the Coriolis parameter, the closure (11) for the mean eddy momentum flux convergence gives a scaling law for the strength of a Hadley cell when its effective Rossby number is small.

c. Climate stability

The regime transition in the scaling of the mean eddy momentum flux convergence and the mean eddy flux of surface potential temperature has implications for the stability of climate with respect to changes in meridional radiative forcing gradients. Consider changes in radiative forcing gradients that are sufficiently small that their effect on the radiative–convective equilibrium static stability, if there is any, can be neglected. In a climate in which baroclinic entropy fluxes modify the extratropical thermal stratification and tropopause height ($S_c \sim 1$), a small change in the radiative forcing gradient is counteracted by a proportionately weak response in the eddy flux of surface potential temperature and, if the effective Rossby number of the Hadley cell is small so that the Hadley cell strength primarily responds to changes in eddy momentum flux divergence, by a proportionately weak response in Hadley cell strength. Conversely, in a climate in which convection and radiation control the extratropical thermal stratification and tropopause height ($S_c < 1$), a small change in the radiative forcing gradient is counteracted by a proportionately stronger response in the eddy flux of surface potential temperature and, if the effective Rossby number of the Hadley cell is small, by a proportionately stronger response in the Hadley cell strength. That is, the proportionate response of the surface potential temperature gradient to a given fractional change in the radiative forcing gradient can be expected to be weaker in a climate in which convection controls the extratropical thermal stratification than in a climate in which baroclinic eddies modify the extratropical thermal stratification. See Zhou and Stone (1993a,b) for a demonstration of this effect for the extratropical climate in a two-layer model.

Assuming these considerations carry over to moist atmospheres, at least qualitatively, one may speculate that a warm climate with sufficiently large convective static stability (e.g., a statically very stable moist adiabat) exhibits a proportionately weaker response to changes in radiative forcing gradients (such as occur, e.g., over the course of a seasonal cycle) than a cold climate with small convective static stability (e.g., a statically neutral dry adiabat). However, effects such as water vapor feedback and changes in the radiative–convective equilibrium static stability in response to radiative forcing changes are likely to complicate any manifestation of such dynamical effects.

d. Relation to previous work

Several aspects of the scaling laws and regime transitions discussed in this paper have previously been discussed in the literature. Green (1970) presented a closure that relates eddy energies to the mean available potential energy. This closure is essentially equivalent to the closure (5) for the regime $S_c \sim 1$. Stone (1972) presented a closure that relates eddy energies to the baroclinic mean kinetic energy. Such a closure does not fit our simulation results well because it gives an incor-

rect dependence of eddy energies on the static stability and on the planetary radius and rotation rate. Both Green and Stone, as well as several subsequent authors, used equipartitioning of eddy energies in closures for atmospheric macroturbulence, with Green arriving at a closure for the eddy flux of potential temperature similar to the closure (9); however, that eddy energies in GCM simulations of a wide range of circulations satisfy equipartitioning relations—with a striking degree of accuracy—has not been demonstrated before. It also appears not to have been noticed before that the ratio of the baroclinic eddy kinetic energy to the other eddy energies depends on the planetary radius and rotation rate.

The importance for macroturbulence closures of modifications of the extratropical thermal stratification by baroclinic entropy fluxes was discussed by Held (1978a,b). Based on quasigeostrophic theory and Stone's (1972) analysis, Held (1978a) argued that the column-integrated eddy flux of potential temperature should depend more strongly on potential temperature gradients when a quasigeostrophic counterpart of the supercriticality satisfies $S_c \ll 1$ than when it satisfies $S_c \gg 1$. This is qualitatively similar to our results, albeit with quantitative differences and with the difference that the limit $S_c \gg 1$ appears unattainable in atmospheric macroturbulence. Based on simulations with a two-layer model on the sphere, Held (1978b) suggested a closure similar to (5) that included an empirical function of a quasigeostrophic supercriticality analogous to our function $\xi(S_c)$. Building on Held's work, Zhou and Stone (1993a,b) demonstrated that modifications of the atmospheric thermal stratification by baroclinic entropy fluxes are important for the scaling of eddy potential temperature fluxes in Lorenz's (1960) two-level model on the sphere. They showed that the scaling of eddy potential temperature fluxes with potential temperature gradients can be in two regimes, depending on whether eddies are or are not allowed to modify the thermal stratification. Held (2007) presented alternative qualitative arguments of how scaling laws of atmospheric macroturbulence can change depending on whether or not baroclinic entropy fluxes modify the extratropical thermal stratification.

e. Limitations and broader applicability

The results presented in this paper have two fundamental limitations. First, the scaling laws we presented are scaling laws for mean values of eddy energies and eddy fluxes. They do not give information on the spatial structure of the fluxes, except for the information that the eddy momentum flux varies meridionally on the energy-containing eddy length scale. For theories of a planet's surface climate and general circulation beyond the level of scaling laws for bulk quantities, information on the horizontal and vertical structure of the eddy fluxes is required. For an energy-balance model for a planet's surface climate, one may attempt to use diffusive closures of the eddy flux of surface potential temperature that are consistent with the scaling laws for mean values of the flux presented in this paper. We have experimented with using the surface potential temperature gradient, smoothed over eddy length scales, as a meridional structure function for the eddy flux of surface potential temperature. Although it appears adequate for qualitative explorations of the dependence of a planet's surface climate on external parameters, such a procedure is not accurate over the entire range of climates we simulated. A more promising (albeit computationally more demanding) approach appears to be to use the weakness of eddy–eddy interactions in turbulence closures that solve for the spatial structure of eddy statistics by a suitable approximation of the hierarchy of moment equations (Marston et al. 2008; O'Gorman and Schneider 2007).

Second, the scaling laws we presented neglect the effects of latent heat release in phase changes of water. An essential question in understanding how latent heat release modifies the scaling laws for dry atmospheres is the question of how the effective static stability experienced by baroclinic eddies is modified. This is an open question (Schneider and O'Gorman 2008). The general consistency of the annual-mean statistics for Earth's atmosphere with the scaling laws and simulation results suggests that the scaling laws may be modified to apply to moist atmospheres. Encouraging results suggesting that aspects of the scaling laws carry over directly to moist atmospheres are presented by O'Gorman and Schneider (2008b), who show that eddy kinetic energies scale with the (dry) mean available potential energy in a range of simulations with an idealized GCM that includes a hydrologic cycle. The reasons for this empirical result and the question of how other aspects of the scaling laws for dry atmospheres can be generalized to moist atmospheres remain to be investigated.

Acknowledgments. We are grateful for support by the Davidow Discovery Fund, by an Alfred P. Sloan Research Fellowship, and by the National Science Foundation (Grant ATM-0450059); for computing resources provided by the National Center for Atmospheric Research (which is sponsored by the National Science Foundation); and for very helpful comments on drafts of this paper by Tim Merlis and Paul O'Gorman. Both the program code for the simulations, based on

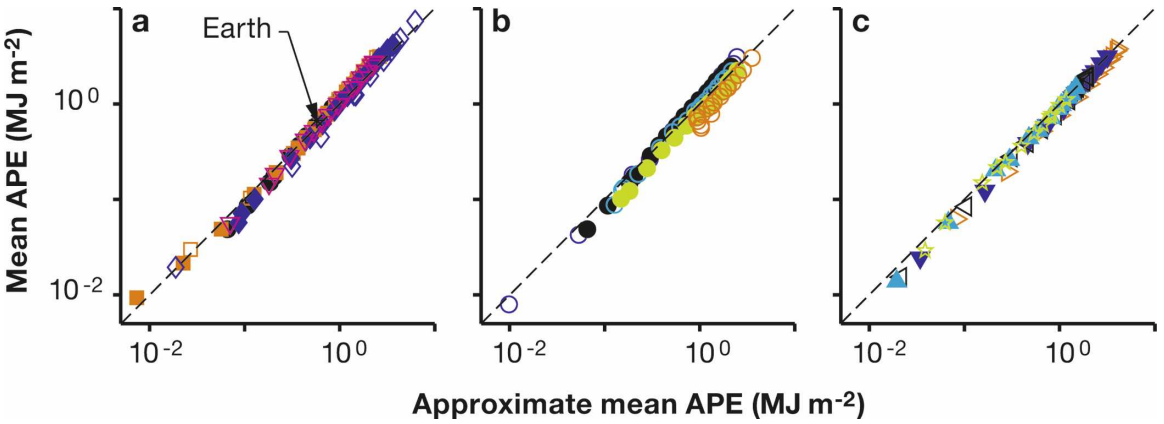

FIG. A1. MAPE (A1) vs approximate MAPE (3). The dashed lines represent the identity MAPE = MAPE_a. Plotting symbols as in Fig. 4.

the Flexible Modeling System of the Geophysical Fluid Dynamics Laboratory, and the simulation results themselves are available from the authors upon request.

APPENDIX A

Approximation of MAPE

The approximate mean available potential energy (3) derives from Lorenz's (1955) quadratic expression for the mean available potential energy in a baroclinic zone,

$$\mathrm{MAPE} = \frac{c_p p_0}{2g} \int_0^1 d\sigma\, \Gamma \left(\frac{\langle \bar{p} \rangle}{p_0} \right)^{\kappa} \left(\langle \bar{\theta}^{\sigma 2} \rangle - \langle \bar{\theta}^{\sigma} \rangle^2 \right), \tag{A1}$$

where

$$\Gamma = -\frac{\kappa}{\langle \bar{p} \rangle} \left\langle \overline{\partial_p \theta}^{\sigma} \right\rangle^{-1} \tag{A2}$$

is an inverse static stability measure and quantities are expressed in sigma coordinates because these are used in the GCM. Taylor expansion of the squared potential temperature variations around the latitude y_0/a of the midpoint of the baroclinic zone, assuming $\bar{\theta}^{\sigma}(y_0) \approx \langle \bar{\theta}^{\sigma} \rangle$ and $\partial_y \bar{\theta}^{\sigma}(y_0) \approx \langle \partial_y \bar{\theta}^{\sigma} \rangle$, gives $\langle \bar{\theta}^{\sigma 2} \rangle - \langle \bar{\theta}^{\sigma} \rangle^2 \approx \langle \partial_y \bar{\theta}^{\sigma} \rangle^2 \langle (y - y_0)^2 \rangle$. Using $\langle (y - y_0)^2 \rangle \approx L_z^2/12$ (which is exact in planar geometry), assuming the contributions to the integral (A1) come from the troposphere, and substituting surface quantities for all interior-troposphere quantities in Eqs. (A1) and (A2), one obtains the approximation MAPE_a given by Eq. (3).

Figure A1 shows that in the simulations, MAPE_a scales with MAPE.[A1] With a few exceptions, MAPE_a does not deviate by more than 25% from MAPE. There is some variation of the ratio MAPE/MAPE_a with the convective lapse-rate parameter γ for simulations with larger surface potential temperature gradients (Fig. A1b). This bias in MAPE_a results because the stabilization of the thermal stratification by baroclinic entropy fluxes is concentrated near the surface, and the thermal stratification in the extratropical upper troposphere ceases to be affected by convection only for larger convective lapse-rate parameters ($\gamma \geq 0.8$) and for the largest surface potential temperature gradients we simulated (SW06; Schneider 2007). Convective lapse rates continue to be found in the extratropical upper troposphere for smaller convective lapse-rate parameters ($\gamma < 0.8$) even when baroclinic entropy fluxes stabilize the lower troposphere. In such cases, the assumption implicit in MAPE_a that the interior-troposphere static stability is approximately equal to (or at least scales with) the near-surface static stability is not accurate. However, the resulting bias in MAPE_a is small enough to be ignorable in this paper. MAPE_a is also a good approximation of MAPE in Earth's atmosphere (Fig. A1a).

Although adequate for our purposes, MAPE_a is not always an adequate approximation of MAPE. When changes in static stability and meridional potential temperature gradients in the interior troposphere do not scale with changes in the corresponding surface quantities, the mean available potential energy (A1) may have to be retained in macroturbulence closures. See

[A1] In Fig. 9, contributions from near the surface and near the top of the model are excluded from the integral (A1); see appendix B.

O'Gorman and Schneider (2008b) for an example involving climate changes in response to changes in the optical thickness of longwave absorbers in an idealized moist atmosphere.

APPENDIX B

Estimation of Flow Statistics

The estimation of flow statistics generally follows appendixes C and D of SW06, with differences as described in what follows.

a. Baroclinic zones

The boundaries of the baroclinic zones over which the meridional mean $\langle\cdot\rangle$ of mean fields is taken are the outermost latitudes at which the eddy flux of potential temperature $\overline{v'\theta'}^{\sigma}\cos(\phi)$ at the near-surface level $\sigma = 0.84$ is 70% of its maximum value. This gives narrower baroclinic zones than those over which meridional means were taken in SW06, where we used a critical value of 30% of the maximum flux to define boundaries of baroclinic zones. The narrower baroclinic zones lead to better fits of the simulation results to the scaling laws in the simulations with $a = 4a_e$ and $\Omega = 4\Omega_e$. The reason appears to be that the narrower baroclinic zones are focused on the dominant jet and that eddy activity in this region dominates the meridionally averaged eddy statistics (see Fig. 1 for an example); including neighboring regions in the meridional mean of mean fields leads to poorer fits. Using wider or narrower baroclinic zones otherwise does not substantially change the results, except for changes in $O(1)$ proportionality factors in the scaling laws. Wider baroclinic zones lead to better fits to the scaling laws in some series of simulations, for example, in those in which the Newtonian relaxation time was varied.

Baroclinic zones can also be determined as regions centered on the barotropic eddy kinetic energy maximum with meridional width equal to the energy-containing length scale L_e. This likewise does not substantially change the results, but the fits of the scaling laws for the simulations with $a > a_e$ and $\Omega > \Omega_e$ are somewhat poorer than those shown in this paper. In this way, the meridional width L_z of the baroclinic zone that enters the approximate mean available potential energy (3) becomes the energy-containing length scale L_e, which could then, as in section 5 and with a further loss of goodness of fit, be approximated by the Rossby radius L_R.

To reduce noise in the results that would be solely due to noise in the determination of baroclinic zones, within each series of simulations with varying Δ_h, we used robust local linear smoothing as in SW06 to ensure smooth variations with Δ_h of the latitudes of the boundaries of the baroclinic zones. The smoothing primarily affects the simulations with smallest Δ_h, for which the Hadley cell extents and the boundaries of baroclinic zones can vary rapidly with Δ_h (Walker and Schneider 2006). Otherwise the effect of the smoothing is minimal. It does not substantially affect the results.

b. Surface averages

Surface or near-surface quantities generally are averages over the near-surface layer between $\sigma = 0.80$ and 0.70, which is immediately above the layer in which boundary layer diffusion of dry static energy strongly affects temperatures. The near-surface eddy flux of potential temperature $\overline{v_s'\theta_s'}$ and the velocity and potential temperature variances used in the calculation of the correlation coefficient c_θ are evaluated at the level $\sigma = 0.84$. The actual surface pressure is used for the quantity p_s.

c. Eddy energies

Eddy energies were estimated as in SW06. As in that paper, levels below $\sigma = 0.9$ and above $\sigma = 0.025$ were not taken into account in the estimation of available potential energies to avoid artifacts due to boundary layer diffusion and due to the rigid-lid upper boundary of the model (at $\sigma = 0$).

d. Tropopause pressure

For the simulations in SW06, the tropopause was determined as in that paper, based on a critical value of the radiative relaxation rate. For the simulations in SchM, the variations in Newtonian relaxation time preclude a determination of the tropopause based on a critical value of the radiative relaxation rate. For those simulations, the tropopause was determined according to the WMO convention as a 2 K km^{-1} isoline of the temperature lapse rate. The results are essentially unchanged if the WMO convention is used to determine the tropopause in all simulations.

e. Eddy length scales

An energy-containing spherical wavenumber was estimated from the barotropic eddy kinetic energy spectrum as in SW06, giving a wavenumber n_e approximately at the peak of the spectrum (see, e.g., Fig. 2). The energy-containing eddy length scale was obtained from the wavenumber via

$$L_e = \frac{\pi a}{\sqrt{n_e(n_e+1)}}. \tag{B1}$$

The Rossby radius was computed (similarly as described in SW06) as

$$L_R = c_R \frac{\langle N_p(\overline{p}_s - \overline{p}_t)\rangle}{f_0} \min(\hat{S}_c, 1), \qquad \text{(B2)}$$

where $N_p^2 = -(\overline{\rho}_s\overline{\theta}_s)^{-1}\overline{\partial_p\theta}^s$ is a near-surface static stability measure and ρ is the density. The reference value of the Coriolis parameter is evaluated at the latitude at which the near-surface eddy flux of potential temperature $\overline{v'\theta'}^{\sigma}\cos(\phi)$ is maximal. The empirical constant is chosen to be $c_R = 1.35\pi$, based on the empirical relation between the Rossby radius (B2) and the energy-containing scale (B1) in SW06.[B1] The supercriticality $\hat{S}_c$ is the supercriticality S_c, evaluated as in SW06 and SchM, but rescaled by dividing the supercriticalities for each series of simulations by the supercriticality of the simulation with largest Δ_h. As mentioned in SW06, this leads to good agreement between the Rossby radius and the energy-containing scale in the simulations in which the planet size does not affect the energy-containing scale.

f. Statistics for Earth's atmosphere

As in SW06, the quantities for Earth's atmosphere included in the figures were computed from reanalysis data for the years 1980–2001 provided by the European Centre for Medium-Range Weather Forecasts (Kållberg et al. 2004; Uppala et al. 2005). The quantities shown are annual means over both hemispheres, averaged in the same manner as the corresponding quantities for the simulations. Eddy fields are fluctuations about annual and zonal means and thus include stationary eddies. The tropopause pressure was determined according to the WMO convention as a 2 K km^{-1} isoline of the temperature lapse rate.

REFERENCES

Andrews, D. G., 1983: A finite-amplitude Eliassen–Palm theorem in isentropic coordinates. *J. Atmos. Sci.,* **40,** 1877–1883.

Charney, J. G., 1971: Geostrophic turbulence. *J. Atmos. Sci.,* **28,** 1087–1095.

Green, J. S. A., 1970: Transfer properties of the large-scale eddies and the general circulation of the atmosphere. *Quart. J. Roy. Meteor. Soc.,* **96,** 157–185.

Held, I. M., 1975: Momentum transport by quasi-geostrophic eddies. *J. Atmos. Sci.,* **32,** 1494–1497.

——, 1978a: The vertical scale of an unstable baroclinic wave and its importance for eddy heat flux parameterizations. *J. Atmos. Sci.,* **35,** 572–576.

——, 1978b: The tropospheric lapse rate and climatic sensitivity: Experiments with a two-level atmospheric model. *J. Atmos. Sci.,* **35,** 2083–2098.

——, 1982: On the height of the tropopause and the static stability of the troposphere. *J. Atmos. Sci.,* **39,** 412–417.

——, 1999: The macroturbulence of the troposphere. *Tellus,* **51A-B,** 59–70.

——, 2007: Progress and problems in large-scale atmospheric dynamics. *The Global Circulation of the Atmosphere,* T. Schneider and A. H. Sobel, Eds., Princeton University Press, 1–21.

——, and D. G. Andrews, 1983: On the direction of the eddy momentum flux in baroclinic instability. *J. Atmos. Sci.,* **40,** 2220–2231.

——, and B. J. Hoskins, 1985: Large-scale eddies and the general circulation of the troposphere. *Advances in Geophysics,* Vol. 28, Academic Press, 3–31.

——, and V. D. Larichev, 1996: A scaling theory for horizontally homogeneous, baroclinically unstable flow on a beta plane. *J. Atmos. Sci.,* **53,** 946–952.

——, and T. Schneider, 1999: The surface branch of the zonally averaged mass transport circulation in the troposphere. *J. Atmos. Sci.,* **56,** 1688–1697.

Ioannou, P., and R. S. Lindzen, 1986: Baroclinic instability in the presence of barotropic jets. *J. Atmos. Sci.,* **43,** 2999–3014.

Kållberg, P., A. Simmons, S. Uppala, and M. Fuentes, 2004: The ERA-40 archive. ECMWF Tech. Rep. 17, 31 pp. [Available online at http://www.ecmwf.int/publications/library/ecpublications/_pdf/era40/ERA40_PRS17_rev1.pdf.]

Koh, T.-Y., and R. A. Plumb, 2004: Isentropic zonal average formulation and the near-surface circulation. *Quart. J. Roy. Meteor. Soc.,* **130,** 1631–1654.

Lee, S., 1997: Maintenance of multiple jets in a baroclinic flow. *J. Atmos. Sci.,* **54,** 1726–1738.

——, 2005: Baroclinic multiple zonal jets on the sphere. *J. Atmos. Sci.,* **62,** 2484–2498.

Lorenz, E. N., 1955: Available potential energy and the maintenance of the general circulation. *Tellus,* **7,** 157–167.

——, 1960: Energy and numerical weather prediction. *Tellus,* **12,** 364–373.

Marston, J. B., E. Conover, and T. Schneider, 2008: Statistics of an unstable barotropic jet from a cumulant expansion. *J. Atmos. Sci.,* **65,** 1955–1961.

O'Gorman, P. A., and T. Schneider, 2007: Recovery of atmospheric flow statistics in a general circulation model without nonlinear eddy–eddy interactions. *Geophys. Res. Lett.,* **34,** L22801, doi:10.1029/2007GL031779.

——, and ——, 2008a: Weather layer dynamics of baroclinic eddies and multiple jets in an idealized general circulation model. *J. Atmos. Sci.,* **65,** 524–535.

——, and ——, 2008b: Energy of midlatitude transient eddies in idealized simulations of changed climates. *J. Climate,* in press.

Panetta, R. L., 1993: Zonal jets in wide baroclinically unstable regions: Persistence and scale separation. *J. Atmos. Sci.,* **50,** 2073–2106.

Pedlosky, J., 1970: Finite-amplitude baroclinic waves. *J. Atmos. Sci.,* **27,** 15–30.

——, 1979: Finite-amplitude baroclinic waves in a continuous model of the atmosphere. *J. Atmos. Sci.,* **36,** 1908–1924.

[B1] The factor π in the empirical constant c_R did not appear in SW06. It appears here for consistency with the factor π in the relation (B1) between length scale and wavenumber, which likewise did not appear in SW06.

Rhines, P. B., 1975: Waves and turbulence on a β-plane. *J. Fluid Mech.,* **69,** 417–443.

Salmon, R., 1980: Baroclinic instability and geostrophic turbulence. *Geophys. Astrophys. Fluid Dyn.,* **15,** 167–211.

——, 1982: Geostrophic turbulence. *Topics in Ocean Physics,* A. R. Osborne and P. M. Rizzoli, Eds., Società Italiana di Fisica, 30–78.

Schneider, T., 2004: The tropopause and the thermal stratification in the extratropics of a dry atmosphere. *J. Atmos. Sci.,* **61,** 1317–1340.

——, 2005: Zonal momentum balance, potential vorticity dynamics, and mass fluxes on near-surface isentropes. *J. Atmos. Sci.,* **62,** 1884–1900.

——, 2006: The general circulation of the atmosphere. *Annu. Rev. Earth Planet. Sci.,* **34,** 655–688.

——, 2007: The thermal stratification of the extratropical troposphere. *The Global Circulation of the Atmosphere,* T. Schneider and A. H. Sobel, Eds., Princeton University Press, 47–77.

——, and C. C. Walker, 2006: Self-organization of atmospheric macroturbulence into critical states of weak nonlinear eddy–eddy interactions. *J. Atmos. Sci.,* **63,** 1569–1586.

——, and P. A. O'Gorman, 2008: Moist convection and the thermal stratification of the extra-tropical troposphere. *J. Atmos. Sci.,* in press.

Smagorinsky, J., S. Manabe, and J. L. Holloway Jr., 1965: Numerical results from a nine-level general circulation model of the atmosphere. *Mon. Wea. Rev.,* **93,** 727–768.

Stone, P. H., 1972: A simplified radiative–dynamical model for the static stability of rotating atmospheres. *J. Atmos. Sci.,* **29,** 405–418.

——, and D. A. Miller, 1980: Empirical relations between seasonal changes in meridional temperature gradients and meridional fluxes of heat. *J. Atmos. Sci.,* **37,** 1708–1721.

Swanson, K. L., and R. T. Pierrehumbert, 1997: Lower-tropospheric heat transport in the Pacific storm track. *J. Atmos. Sci.,* **54,** 1533–1543.

Thuburn, J., and G. C. Craig, 2000: Stratospheric influence on tropopause height: The radiative constraint. *J. Atmos. Sci.,* **57,** 17–28.

Tung, K. K., 1986: Nongeostrophic theory of zonally averaged circulation. Part I: Formulation. *J. Atmos. Sci.,* **43,** 2600–2618.

Uppala, S. M., and Coauthors, 2005: The ERA-40 re-analysis. *Quart. J. Roy. Meteor. Soc.,* **131,** 2961–3012.

Vallis, G. K., 2006: *Atmospheric and Oceanic Fluid Dynamics: Fundamentals and Large-scale Circulation.* Cambridge University Press, 771 pp.

Walker, C. C., and T. Schneider, 2006: Eddy influences on Hadley circulations: Simulations with an idealized GCM. *J. Atmos. Sci.,* **63,** 3333–3350.

Zhou, S., and P. H. Stone, 1993a: The role of large-scale eddies in the climate equilibrium: Part I: Fixed static stability. *J. Climate,* **6,** 985–1000.

——, and ——, 1993b: The role of large-scale eddies in the climate equilibrium: Part II: Variable static stability. *J. Climate,* **6,** 1871–1880.